Optics Letters

Maskless nanostructure photolithography by ultrahigh-order modes of a symmetrical metal-cladding waveguide

Meng Zhang,[1] Hailang Dai,[1,*] Yuxi Shang,[1] Zhuangqi Cao,[1] and Xianfeng Chen[1,2,3,4]

[1] State Key Laboratory of Advanced Optical Communication Systems and Networks, School of Physics and Astronomy, Shanghai Jiao Tong University, Shanghai 200240, China
[2] Shanghai Research Center for Quantum Sciences, Shanghai 201315, China
[3] Collaborative Innovation Center of Light Manipulations and Applications, Shandong Normal University, Jinan 250358, China
[4] e-mail: xfchen@sjtu.edu.cn
*Corresponding author: hailangdai@sjtu.edu.cn

Received 21 October 2021; revised 14 November 2021; accepted 15 November 2021; posted 15 November 2021; published 19 December 2021

To fabricate fine patterns beyond the diffraction limit, a nanostructure photolithography technique is required. In this Letter, we present a method that allows sub-100-nm lines to be patterned photolithographically using ultrahigh-order modes from a symmetrical metal-cladding waveguide (SMCW) in the near field, which are excited by continuous-wave visible light without focusing. The etching depth of the nanopattern reaches more than 200 nm. The localized light intensity distribution can be used to map the photoresist exposure pattern, which agrees well with our theoretical model. This technique opens up the possibility of localizing light fields below the diffraction limit using maskless and lower power visible light.

https://doi.org/10.1364/OL.446431

Photolithography technology is one of the key drivers of our modern scientific and technological society. It has many applications in integrated circuit fabrication [1,2], microelectronics [3–5], and micro-nanofabrication [6–8]. The miniaturization of microelectronics and optoelectronic devices using advanced nanoscale photolithography technology have received interest for applications such as nanostructured chips [9], metasurfaces [10], and photonic crystals [11]. Therefore, to achieve a nanoscale lithography technology that can break through the limitations of existing technology is an irresistible target with the rapid development of science and technology. We know that the linewidth and etching depth of nanopatterns are significant indicators of photolithography technology, and the final aim of research in this field is to obtain a nanolithography technology that is cost-effective and produces a narrow linewidth. The linewidth in photolithography can be controlled by the numerical aperture and the wavelength of the light source [12], and the etching depth is closely related to the energy of the light beam. Therefore, there are two ways to achieve a narrower linewidth in photolithography technology: by reducing the light wavelength and increasing the numerical aperture. These two methods lead to a smaller focusing spot and weaker diffraction limitation. However, the ability to increase the numerical aperture is limited due to current limitations of engineering technology. Reducing the wavelength of the light source has therefore become the main way to obtain a narrower photolithographic linewidth. Many micro-nanofabrication techniques have emerged, such as extreme ultraviolet lithography [13,14], focused ion beam lithography [15,16], electron beam exposure lithography [17–20], X-ray lithography [21,22], and immersion lithography [23]. Another major class of methods use a structural light field in which the light energy is confined to a very small-scale light spot to expose the photoresist. For example, Luo [24] used grating structures to excite a surface plasmon polariton (SPP) that was locally exposed on the photoresist surface, achieving a 1/9-wavelength surface plasmon (SP) interference pattern. However, for extreme ultraviolet lithography and electron beam lithography, high-power light sources are generally difficult to obtain, and they all require high-vacuum conditions. Moreover, in structured light field lithography, although the evanescent field has a narrow spectrum, the depth of the lithographic pattern is insufficient.

In this letter, we demonstrate a method that utilizes ultrahigh-order modes (UOMs) in an SMCW for nanoscale photolithography, as shown in Fig. 1. UOMs have a narrow linewidth and a high power density in the mode oscillating zone [25]. Meanwhile, the effective refractive index of the SMCM is very small due to the small incident angle, which indicates that the group velocity of the UOMs is close to zero in the transmission direction. Hence, the coupled light is confined to a small zone, which causes coherent oscillation in the guiding layer, resulting in an enhancement of the oscillation field in the small coherent oscillation zone. Because the UOM group velocity v_g is close to 0, the oscillation zone is small in the transmission direction. The linewidth of the guided mode resonance with high energy density can reach the nanoscale, enabling the diffraction limit to be broken. Therefore, we have designed a system and an experimental setup to demonstrate the linewidth and etching depth of UOM nanoscale photolithography technology with experimental data.

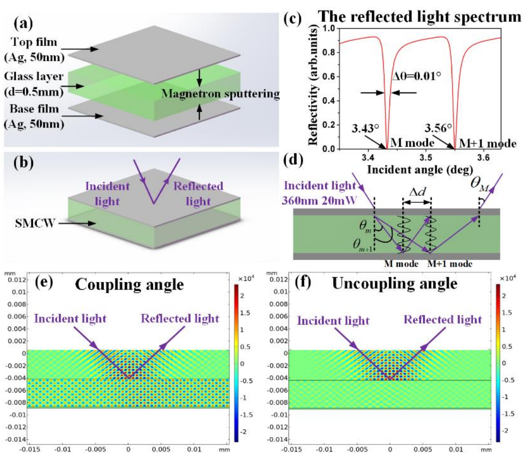

Fig. 1

Fig. 1. (a) Schematic of the SMCW chip. (b) Continuous-wave (CW) light is directed nearly vertically onto the SMCM. (c) Calculated reflectivity of the UOMs versus the incident angle, as obtained using ATR software; the simulation parameters are given in Supplement 1. (d) Distribution of fields in the waveguide layer of the SMCW chip. (e) and (f) Results from COMSOL simulations of the SMCW when the incident light is at the coupling angle and when it is not, respectively (more details are provided in Supplement 1).

In the numerical simulation and experimental setup, the SMCW ($14 \times 14 \times 0.50\,\text{mm}^3$) included a thin silver film as the coupling layer (50 nm thick) on the top, a glass slab as the guiding layer (0.50 mm thick) in the middle, and a silver film as the substrate layer (50 nm thick) at the bottom. The parallelism of the upper and lower surfaces of the glass slab was less than 4″, as shown in Fig. 1(a). The incident light irradiated the top of the waveguide at a very small incident angle θ (less than 5°), as shown in Fig. 1(b). When the incident angle matched the coupling angle, the incident light was coupled into the guiding layer of the SMCW. Figure 1(c) plots the attenuated total reflection (ATR) peaks obtained from numerical simulations [26,27]. The UOMs were ultimately excited under the wave-vector-matching condition by free-space coupling technology [26], resulting in a high-power-density standing wave field in the guiding layer of the SMCW, as shown in Fig. 1(d).

We analyzed the linewidth and etching depth of UOM photolithography technology according to electromagnetic field theory. In the SMCW, the propagation constant of the excitation mode is $\beta = k_0 n_1 \sin\theta$, where $n_1 = 1.4$ is the refractive index of the glass slab and θ is the angle of the incident light. The effective refractive index of the waveguide is $N_{eff} = \beta/k_0$. When $\theta \to 0$, the group velocity of the UOMs in the transmission direction (transverse), $v_g = \frac{d\omega}{d\beta} = \frac{N_{eff}}{n_1} \times \frac{c}{(n_1+\omega dn_1/d\omega)}$, is approximately zero in the longitudinal direction, as shown in Fig. 1(d). Therefore, the UOMs only oscillate between the metal-cladding layers of the SMCW without scattering in the transmission direction. The energy of the modes is confined to a small zone, which causes a high-energy-density standing wave field to form in the guiding layer. According to the eigenvalue equation of the model in the numerical simulation [28], the number of modes m can reach more than 10^3.

To describe the field distribution in the waveguide layer, the model of the waveguide layer in the structure was numerically simulated by COMSOL software, as shown in Figs. 1(e) and 1(f). The incident light had a wavelength of 360 nm and a Gaussian profile. We selected the coupling angle as the incident angle using the ATR software. The simulation results show that the light is coupled into the guiding layer of the SMCW and induces a standing wave field due to coherent resonance. When the incident angle reaches the coupling angle, the incident light is coupled into the guiding layer and forms a high-energy-density standing wave field in a small zone. There is no standing wave field in the guiding layer unless the incident angle reaches the coupling angle, as shown in Figs. 1(e) and 1(f). According to the numerical simulations, the UOMs of the SMCW have the ability to achieve nanometer linewidth and deeply etched patterns on the base.

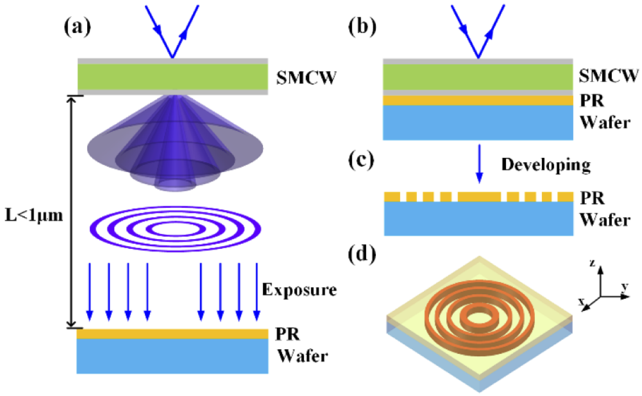

Fig. 2. Schematic of the UOM photolithography system. (a) Transmitted light cones formed by leakage radiation from the UOMs. (b) Photoresist (PR) is subjected to UOM exposure. (c) After exposure, the photoresist is developed. (d) Schematic of the photolithography pattern.

A schematic of the UOM photolithography process is shown in Fig. 2. When the coupling angle is reached, the incident light is coupled into the guiding layer of the SMCW. The transmitted light cones formed by leakage radiation and the optical intensity in the guiding layer are enhanced compared with the incident light, as shown in Fig. 2(a). The projection of the light cones into the x–y plane, where the photoresist is located, forms concentric rings. Figure 2(b) shows that the photoresist (AR-P 3700) was spun onto a substrate consisting of a 1-mm-thick treated glass wafer, followed by hot plate tempering at 100 °C for 60 s. The exposure light source was a continuous-wave laser with a wavelength of 360 nm and a power of 20 mW. After being exposed for 60 s, the sample was soaked in a developer (AR 300-47, main component TMAH, Germany) for 40 s and then rinsed with deionized water for 30 s.

The distance between two patterns Δd and the linewidth of UOM photolithography Δl was calculated in detail by analyzing the structure of the system as follows. The separation of the maximum intensity position is determined by the two adjacent UOMs. The position of maximum exposure intensity corresponds to the position of lowest reflected light intensity, and the distance between photolithographic lines can be obtained by calculating the spacing of modes. As shown in Fig. 1(d), θ_M is the reflected angle of the mth mode in air, and θ_{m+1} and θ_m are the transmission angles of the mth and $(m+1)$th modes, respectively. The distance between the two patterns Δd is approximately equal to $\Delta d = h(\tan\theta_{m+1} - \tan\theta_m)$. According to the Snell formula, we

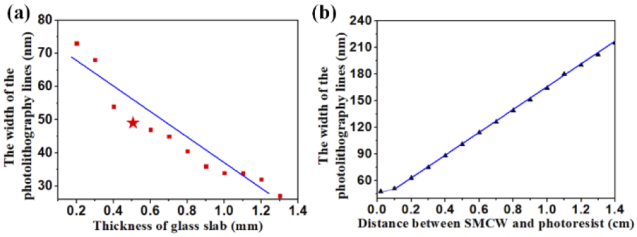

Fig. 3. (a) Plot of the change in the width of the photolithography lines Δl with the thickness of the glass slab. (b) Plot of the change in the width of the photolithography lines Δl with the distance between the SMCW and photoresist.

found that

$$\Delta d = d(\tan \arcsin(\sin(\theta_{M+1})/n_1) - \tan \arcsin(\sin(\theta_M)/n_1)). \quad \textbf{(1)}$$

In Fig. 1(c), two resonance dips corresponding to two ultrahigh-order modes can be observed, where θ_M and θ_{M+1} are 3.43° and 3.56°, respectively. According to Eq. (1), the separation generated by two adjacent modes is about 1.0 µm. We can see that the full width at half maximum (FWHM) of the mth mode is equal to the linewidth of UOM photolithography. The eigenequation of the SMCW modes is $\kappa d = m\pi + 2 \arctan\left(\frac{\alpha}{\kappa}\right)$, where $k_0 = \frac{2\pi}{\lambda}$ is the free-space wavenumber, $\kappa = (k_0^2 n_1^2 - \beta^2)^{\frac{1}{2}}$, and $\alpha = (\beta^2 - k_0^2 n_2^2)^{\frac{1}{2}}$. From the above derivation, we can obtain the linewidth of UOM photolithography Δl as

$$\Delta l = \left[\frac{m\pi}{k_0 n_1 \cos\theta} + 2 \arctan\left(\frac{|n_1^2 \sin^2\theta - n_2^2|^{\frac{1}{2}}}{n_1 \cos\theta}\right)\right] \times \Delta\theta. \quad \textbf{(2)}$$

According to Eq. (2), the linewidth of UOM photolithography Δl is about 49 nm when the thickness of the guiding layer is 0.5 mm. We used ATR software to obtain the reflectivity of the UOMs with different thicknesses of the guiding layer with respect to the incident angle of SMCW, and obtained the change in Δl with d by numerical calculation, as shown in Fig. 3(a). It can be seen that the width of the photolithography lines is about 49 nm when the thickness of the guiding layer is 0.5 mm. Due to the presence of laser diffraction, the distance between the SMCW and photoresist (L) will affect the width of the photolithography lines, as shown in Fig. 3(b).

The experimental system is shown in Fig. 4(a). A collimated beam from a diode-pumped solid-state (DPSS) laser (wavelength 360 nm, 20 mW, continuous wave (CW), spot diameter 1 mm) passed through apertures and an expander and then irradiated the SMCW chip. Meanwhile, the chip was fixed onto a step-motor-controlled $\theta/2\theta$ goniometer. The laser beam was expanded through a beam expander and an aperture to obtain a collimated light beam. The $\theta/2\theta$ goniometer was an incident-angle-regulating device that was used to adjust the angle between the SMCW and the incident light. A photoelectric detector (PD) was used to detect the reflected intensity of the modes.

When the incident angle matched a certain mode in the SMCW, the incident light was almost completely coupled into the waveguide, exciting a series of strong cavity modes. A series of concentric rings were seen at the transmission screen, as shown in Fig. 4(b). The physical principle of the formation of a light cone in the transmission direction is that when the incident angle matches a certain mode in the waveguide, the light energy

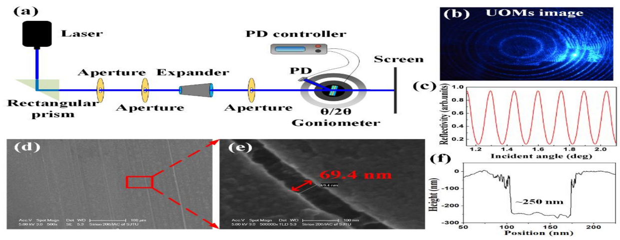

Fig. 4. (a) Schematic of the experimental setup. (b) Image of the light cones on a screen in the transmission direction. (c) Our experimental system detected ATR peaks representing the reflected intensity of the modes versus the incident angle. (d) SEM image of stripes fabricated by UOM photolithography. (e) The region corresponding to the square in Fig. 4(d) magnified 100 times, showing a linewidth of less than 70 nm. (f) The etching depth of the nanopattern reached approximately 250 nm.

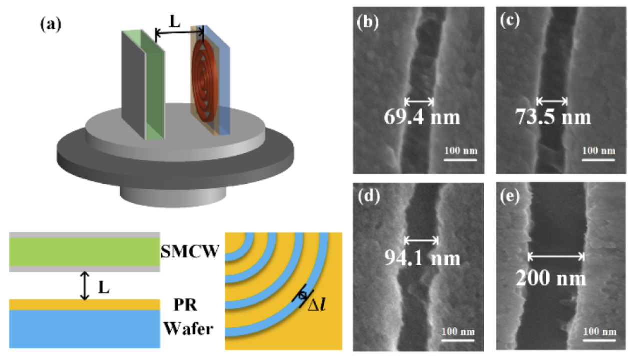

Fig. 5. (a) SMCW and photoresist are fixed onto the $\theta/2\theta$ goniometer, the rotation of which is controlled by a PC. The distance between the SMCW and photoresist is L, and the width of a stripe is Δl. (b) and (c) SEM images: $L < 1$ µm, $\Delta l \sim 70$ nm. (d) SEM image: $L \approx 0.3$ cm, $\Delta l \sim 94$ nm. (e) SEM image: $L \approx 1.1$ cm, $\Delta l \sim 200$ nm.

is coupled into the waveguide for transmission. As the metallic layer is relatively thin, all the UOMs become leaky modes. A concentric light cone can be observed for each UOM with a fixed transverse wave vector, as its energy is transferred back to free space through leakage radiation. That is to say, after the incident light is coupled and stored in the guiding layer, leakage radiation is produced via all UOM channels, while each mode leakage produces a reflection cone. Hence, we observe a series of concentric cones in the experiment. The experimentally measured coupling efficiency was more than 87%, as shown in Fig. 4(c). After performing the photolithography process shown in Fig. 2, we obtained a series of photolithography lines, as shown in Fig. 4(d) and, magnified 10^2 times, in Fig. 4(e). These sub-70-nm-wide and 250-nm-deep photolithography lines were successfully created by a 360 nm CW laser. This result is consistent with the result of theoretical calculations using Eq. (2). After magnifying the SEM image, owing to the limited field of view, only one pattern can be seen (Scanning Electrical Microscope, Sirion 200).

According to the experiment and theory, the linewidth of UOM photolithography Δl in our method is related to the distance L between the photoresist and the SMCW chip, as shown in Fig. 5(a). We adjusted the light path and observed the ATR spectrum, and the incident light was coupled into the waveguide at the coupling angle. Then, the photoresist-coated wafer was placed

Table 1. Calculated and Experimentally Determined Variation of Δl with the Distance L

Distance between SMCW and Photoresist (L)	$L < 1$ μm	0.3 cm	1.1 cm
Calculated Δl	~49 nm	~85 nm	~180 nm
Experimentally Determined Δl	~70 nm	~94 nm	~200 nm

on the $\theta/2\theta$ goniometer. The distance L between the SMCW and the photoresist-coated wafer was adjusted from far to near ($L = 1$ μm, 0.3 cm, and 1.1 cm). After 60 s of exposure followed by 40 s of development in the developer, we obtained the photolithography patterns shown in the SEM images of Figs. 5(b)–5(e) and in Table 1. Upon analyzing the experimental data, when the distance L was less than 1 μm, the width Δl of the photolithography lines was about 70 nm; see the SEM images shown in Figs. 5(b) and 5(c). When the distance L was approximately 0.3 cm, the width Δl of the photolithography lines was about 100 nm; see the SEM image shown in Fig. 5(d). When the distance L was approximately 1.1 cm, the width Δl of the photolithography lines was about 200 nm, as shown in Fig. 5(e). The experimental results are also displayed in Table 1 and Fig. 3(b).

In summary, we have demonstrated a photolithography method that can create a sub-70-nm-wide linewidth and a 250 nm etching depth of photolithography exposed by a 360 nm CW laser. The feasibility of the proposed method has been confirmed theoretically and experimentally. Meanwhile, the linewidth of photolithography can be controlled by adjusting the distance between the waveguide and the photoresist and by changing the thickness of the guiding layer. This method does not need to be performed in a vacuum environment or with an EUV light source, so it is an inexpensive and easy-to-implement method for potentially achieving maskless nanostructure photolithography.

Funding. Foundation for Shanghai Municipal Science and Technology Major Project (2019SHZDZX01-ZX06); China Postdoctoral Science Foundation (2020M681275, 2021T140452); National Natural Science Foundation of China (11734011, 11764020, 12104298); National Key Research and Development Program of China (2018YFA0306301).

Disclosures. The authors declare no conflicts of interest.

Data availability. Data underlying the results presented in this paper are not publicly available at this time but may be obtained from the authors upon reasonable request.

Supplemental document. See Supplement 1 for supporting content.

REFERENCES

1. C. Probst, C. Meichner, K. Kreger, L. Kador, C. Neuber, and H. W. Schmidt, Adv. Mater. **28**, 2624 (2016).
2. A. Santos, M. J. Deen, and L. F. Marsal, Nanotechnology **26**, 042001 (2015).
3. R. Seisyan, Tech. Phys. **56**, 1061 (2011).
4. B. Duong, P. Gangopadhyay, J. Brent, S. Seraphin, R. O. Loutfy, N. Peyghambarian, and J. Thomas, ACS Appl. Mater. Interfaces **5**, 3894 (2013).
5. Y. Cao and M. Gu, Appl. Phys. Lett. **103**, 213104 (2013).
6. J. Liu, M. Ashmkhan, G. Dong, B. Wang, and F. Yi, Sol. Energy Mater. Sol. Cells **108**, 93 (2013).
7. Y. H. Sung, Y. D. Kim, H.-J. Choi, R. Shin, S. Kang, and H. Lee, Appl. Surf. Sci. **349**, 169 (2015).
8. M. Gonidec, M. M. Hamedi, A. Nemiroski, L. M. Rubio, C. Torres, and G. M. Whitesides, Nano Lett. **16**, 4125 (2016).
9. R. Zhang, D. Huang, Y. Y. Fan, X. Liu, and J. Chu, J. Micromech. Microeng. **31**, 085008 (2021).
10. J. Luo, Z. Bo, C. Wang, G. Ping, K. Liu, M. Pu, J. Jin, Z. Zhao, L. Xiong, and H. Yu, Nanoscale **7**, 18805 (2015).
11. S. K. Selvaraja, P. Jaenen, W. Bogaerts, D. V. Thourhout, and R. Baets, J. Lightwave Technol. **27**, 4076 (2009).
12. M. Khorasaninejad, W. T. Chen, R. C. Devlin, J. Oh, A. Y. Zhu, and F. Capasso, Science **352**, 1190 (2016).
13. P. D. Ashby, D. L. Olynick, D. F. Ogletree, and P. P. Naulleau, Adv. Mater. **27**, 5813 (2015).
14. M. C. Marconi and P. W. Wachulak, Prog. Quantum Electron. **34**, 173 (2010).
15. J. P. Adam, J. P. Jamet, J. Ferré, A. Mougin, S. Rohart, R. Weil, E. Bourhis, and J. Gierak, Nanotechnology **21**, 445302 (2010).
16. S. Ahn, S. Kim, and H. Jeon, Appl. Phys. Lett. **96**, 131101 (2010).
17. C. Vieu, F. Carcenac, A. Pépin, Y. Chen, M. Mejias, A. Lebib, L. Manin-Ferlazzo, L. Couraud, and H. Launois, Appl. Surf. Sci. **164**, 111 (2000).
18. C. Joachim, J. K. Gimzewski, and A. Aviram, Nature **408**, 541 (2000).
19. P. B. Fischer and S. Y. Chou, Appl. Phys. Lett. **62**, 2989 (1993).
20. J. A. Sang, M. Kaholek, W. K. Lee, B. L. Mattina, T. H. Labean, and S. Zauscher, Adv. Mater. **16**, 2141 (2004).
21. J. R. Maldonado and M. Peckerar, Microelectron. Eng. **161**, 87 (2016).
22. C. Cuisin, A. Chelnokov, J. M. Lourtioz, D. Decanini, and Y. Chen, Appl. Phys. Lett. **77**, 770 (2000).
23. R. Dammel, F. M. Houlihan, R. Sakamuri, D. Rentkiewicz, and A. Romano, J. Photopolym. Sci. Technol. **17**, 587 (2004).
24. X. G. Luo and T. Ishihara, Appl. Phys. Lett. **84**, 4780 (2004).
25. L. Chen, Z. Cao, F. Ou, H. Li, Q. Shen, and H. Qiao, Opt. Lett. **32**, 1432 (2007).
26. H. Li, Z. Cao, H. Lu, and Q. Shen, Appl. Phys. Lett. **83**, 2757 (2003).
27. Y. Zheng, Z. Cao, and X. Chen, J. Opt. Soc. Am. A **30**, 1901 (2013).
28. H. Lu, Z. Cao, H. Li, and Q. Shen, Appl. Phys. Lett. **85**, 4579 (2004).